sustainability

MDPI

Article

Exploring the Interaction Between Landslides and Carbon Stocks in Italy

Jibran Qadri and Francesca Ceccato *

Department of Civil, Environmental and Architectural Engineering (DICEA), University of Padova, Via Ognissanti, 39, 35129 Padova, Italy; jibran.qadri@studenti.unipd.it
* Correspondence: francesca.ceccato.1@unipd.it; Tel.: +39-049-827-7991

Abstract: Landslides, as natural hazards, have far-reaching impacts beyond their immediate effects on human lives and infrastructure; landslides disrupt both carbon storage and ecosystem stability, and their role in the global carbon cycle cannot be underestimated. This study delves into the complex relationship between landslides and carbon stocks such as, in particular, soil organic carbon (SOC) and above-ground biomass (AGB), and outlines the spatial relationship between different types of landslides, soil organic carbon (SOC), and the carbon cycle, underscoring the importance of understanding these interconnections for environmental sustainability and climate change mitigation efforts. By employing machine learning algorithms on the Google Earth Engine platform, landslide susceptibility maps were created for different landslide types across Italy, and their spatial patterns with SOC accumulation were analyzed using the Python environment. The findings reveal a nuanced relationship between landslide hazard levels and SOC dynamics, with varying trends observed for different landslide types. In addition, this study investigates the potential impact of large-scale landslide events on carbon sequestration in the short term via a case study of the May 2023 landslide event in the Emilia Romagna region of Italy. The analysis reveals a substantial reduction in above-ground biomass by 35%, which approximately accounts for the loss of 0.133 MtC, and a decrease in SOC accumulation in 72% of the affected areas, indicating that landslides can transform carbon sinks into carbon sources, at least in the short term, and suggested that carbon released from extreme landslide events at a larger scale needs to be accounted for in regional or national carbon emissions. This research underscores the importance of considering landslides in carbon cycle assessments and emphasizes the need for sustainable land management strategies to protect and enhance carbon sinks, such as forests and healthy soils, in the face of increasing natural hazards and climate change impacts.

Keywords: landslide susceptibility map; machine learning; soil organic carbon; above-ground biomass; risk assessment; carbon stocks

Citation: Qadri, J.; Ceccato, F. Exploring the Interaction Between Landslides and Carbon Stocks in Italy. *Sustainability* **2024**, *16*, 11273. https://doi.org/10.3390/su162411273

Academic Editor: Maurizio Lazzari

Received: 24 October 2024
Revised: 10 December 2024
Accepted: 16 December 2024
Published: 23 December 2024

1. Introduction

Landslides are natural hazards that can pose significant threats not only to human lives but also to ecosystems and can potentially become sources of carbon dioxide (CO_2) emissions. These mass movements of rock, debris, or earth down a slope can cause extensive damage to vegetation and disrupt soil cover, leading to various physical, chemical, and biological changes. Landslides can release soil organic carbon (SOC) stored in the soil and vegetation, contributing to increased atmospheric CO_2 levels [1,2]. SOC plays a crucial role in the global carbon cycle, acting as both a source and sink of atmospheric CO_2 through processes like photosynthesis, decomposition, and respiration [3–7]. However, both natural factors, like landslides and floods, and human activities like deforestation, agriculture, and urbanization often deplete this essential carbon pool [8]. Sustainable land management practices that promote SOC conservation and enhance carbon sequestration in soils, are critical for mitigating climate change and reducing anthropogenic CO_2 emissions [9].

Previous research suggests that landslides can act as both carbon sources and sinks, but their overall impact on the carbon cycle remains poorly understood. Some studies indicate that landslides can bury and sequester carbon by exposing carbon-rich subsoils and creating new spaces for vegetation growth [10–14]. However, other findings suggest that large-scale landslide events can release substantial amounts of stored carbon from soils and vegetation, potentially turning carbon sinks into sources [15]. Landslide deposits exhibit significant variability in soil properties, particularly in soil organic carbon (SOC), a critical component of global carbon cycling [16]. Soils in landslide scars are particularly vulnerable, with accelerated decomposition rates similar to those seen in surficial soil erosion [17,18]. This disruption extends to chemical and biochemical properties, emphasizing SOC's critical role in soil recovery and ecosystem restoration [19]. Forests are central to global carbon storage, holding 62–78% of terrestrial carbon, with 70% of this stored in soil [20]. Soil organic matter, a primary contributor to forest carbon stocks, ranks second only to above-ground biomass [21]. Yet, disturbances like deforestation and landslides lead to substantial carbon emissions and hinder reclamation, which is often slow due to long-term effects on SOC and nutrient availability [22,23]. The restoration of landslide-affected areas remains a challenge. Artificial restoration has been shown to yield immediate benefits for SOC recovery, but its long-term effects align with those of natural regeneration [24,25]. Effective forest management strategies, as discussed by Pang et al. (2024) [26], could enhance forest health and biodiversity, aiding carbon sequestration. Furthermore, Di et al. (2023) [27] emphasize the significance of landslide scale, particularly width, in determining SOC dynamics and the potential for post-disaster recovery.

Pandey Hari et al. (2022) [28] studied the recovery of vegetation after the landslides triggered by the 2015 Gorkha earthquake and found that by 2022, about 51% of the lost vegetation had been restored. Of this, only 9.5% was due to human-led restoration efforts, with the majority of regrowth occurring naturally. Their analysis suggests that it will take at least sixteen years for the vegetation to fully return to pre-landslide levels, highlighting the resilience of the ecosystem but also the long-term nature of recovery after such disasters.

In recent studies like the Fiordland region, multiple regional landslide events influenced carbon storage significantly. According to the study [29], such events should be included in national greenhouse gas inventories, and another study reveals that each large earthquake can erode millions of tonnes of carbon [30], highlighting the long-term impact of such disturbances on carbon export from mountain forests. Landslides significantly impact both carbon storage and ecosystem stability, making their role in the global carbon cycle critically important.

Most of the studies in the literature have focused on individual landslides, small regions [16], or earthquake-induced landslides over large areas [28,29]; this paper investigates the impact of rainfall-triggered landslides over a large region, which is a novelty in the literature, and contributes to advancing our understanding of the broader implications for the carbon cycle.

The purpose of this paper is to explore the interaction between landslides and carbon stocks, specifically soil organic carbon (SOC) and above-ground biomass (AGB). While it is well established that vegetation can reduce landslide susceptibility by improving soil stability and slope reinforcement through root systems [31,32], there is a lack of comprehensive studies analyzing the relationships between SOC and landslide hazard levels across different landslide types. This study aims to explore the spatial patterns between SOC accumulation and landslide susceptibility classes, providing insights into how SOC dynamics may influence or be influenced by different types of landslide events. To the authors' knowledge, this is a novelty in the literature. Understanding these relationships is important for sustainability as it highlights the interconnections between carbon stocks, natural hazards, and their potential impacts on climate change mitigation efforts.

Landslide susceptibility mapping (LSM) is a spatial tool employed to assess the probability of landslide occurrence and identify areas most vulnerable to such events within a given study region [33]. This mapping technique typically incorporates various causative

factors that influence landslide occurrence, encompassing geological, hydrological, ecological, geomorphological, and anthropogenic variables. These factors may include, but are not limited to, precipitation patterns, land cover characteristics, and topographical slope.

Random Forest, a machine learning algorithm, has emerged as a particularly effective method for landslide susceptibility analysis. Its capacity to process large datasets and manage numerous variables simultaneously, coupled with its robustness against multicollinearity issues, renders it an advantageous choice for landslide studies [34]. This algorithm's ability to handle complex, multidimensional data makes it well suited for the intricate nature of landslide susceptibility assessment, which often involves the integration of diverse geospatial and environmental parameters.

Various types of landslides, such as rainfall-triggered (RT), slow (SL), complex (C), rotational/translational (RT), shallow (SH), fall (F), rapid (R), diffused fall (DF), and Deep-Seated Gravitational Slope Deformations (DSGSDs), were considered according to the distinction used in Table 1, which shows the Italian Landslide Inventory (IFFI). The definition of each landslide type is any given machine learning algorithm for landslide susceptibility mapping that uses 18 parameters derived from a digital elevation model (DEM) and satellite data. IFFI and ITALICA [35,36] catalogs (https://doi.org/10.5281/zenodo.8009366) are used for model training and testing. The landslide susceptibility map is used together with the SOC map available on GEE by OpenLandMap to identify patterns between landslide hazard levels and SOC. This is a novelty in the literature, and even if temporal changes in LS and SOC are not included, and despite the limitations deriving from the use of satellite data, it is meaningful to provide insights into the complex interplay between landslides, SOC dynamics, and their potential impacts on the carbon cycle and climate change mitigation strategies. We hypothesized that the influence on SOC and carbon stocks if landslides occur in the future, through patterns, could be instrumental in understanding the relative impact of different types of landslides on carbon stocks, and the pilot case of the May 2023 landslides in Emilia Romagna, Italy, is used to support this hypothesis.

Table 1. Definition of landslide types.

Name	Definition	Figure
Rapid Flow (R)	This can be characterized by the fast movement of debris, often resembling a fluid-like motion. These landslides can occur in various forms, including debris flows, mudflows, and avalanches, depending on the composition and fluidity of the material involved [37,38].	 (modified from [39])
Fall (F)	Falls are landslides in which the fall of rock or debris occurs through free-fall motion. This type typically involves detached blocks of rock or soil that plunge or tumble downward due to gravitational forces. Falls often occur on steep slopes and are triggered by factors such as weathering, seismic activity, or erosion [40].	 (modified from [41])

Table 1. *Cont.*

Name	Definition	Figure
Shallow (SH)	Shallow landslides occur within the upper layers of the slope, typically involving only a small depth of soil or rock material. These landslides often result from the failure of surface materials due to factors such as saturation, erosion, or changes in slope stability [38].	 (modified from [42])
Complex (C)	These landslides involve more than one failure mechanism occurring simultaneously or sequentially, making them multifaceted in nature. This type often includes a combination of sliding, flowing, and falling components [40].	 (modified from [43])
Rainfall-Triggered Landslide (RT)	Rainfall-triggered landslides are those induced or exacerbated by precipitation events. Heavy or prolonged rainfall can increase the pore water pressure within the slope material, reducing its shear strength and leading to slope failure. Rainfall-triggered landslides can induce both rapid flows (such as debris flows) and slow flows (such as creep or slumps) depending on the intensity and duration of the rainfall event and the characteristics of the slope material.	 (modified from [44])
Diffused Fall (DF)	This category combines characteristics of falls and topples but is used when the precise initiation mechanism is unclear. It refers to landslides where the debris is evident, but the exact cause of the fall or topple cannot be distinctly identified, resulting in a generalized classification [45].	 (modified from [46])
Slow Flow (SL)	These landslides involve the gradual movement of material, usually containing clay, which moves slowly down a slope. This type includes non-liquefied flows of materials such as sand, silt, gravel, debris, and instances of lateral spreading [38].	 (modified from [47])

Table 1. *Cont.*

Name	Definition	Figure
Deep-Seated Landslides (DSGSDs)	These are characterized by their deep slip surfaces, often occurring within large volumes of soil or rock. They are typically slow-moving and involve significant depths below the surface, affecting large land areas [48].	 (modified from [49])
Translational/Rotational Landslides (TR)	These involve the downslope movement of material along a relatively planar surface. Translational landslides can include both translational sliding, where the material moves parallel to the slope, and rotational sliding, where the movement occurs along a curved surface, causing the sliding mass to rotate [38].	 (modified from [43])

A case study of a big disaster event of landslides in Emilia Romagna (Italy) [50], which occurred in May 2023, is analyzed to evaluate the impact on vegetation and carbon storage. More than 60 thousand landslides of different typologies occurred and were mapped with polygons, over which the changes in NDVI and above-ground biomass is analyzed. This quantitative study proves that landslides reduce carbon sequestration and increase potential carbon release into the atmosphere, contributing to increased CO_2 levels, at least in the short term. This highlights the importance of considering landslides in carbon cycle assessments, especially as climate change induces more extreme weather events, potentially turning carbon-absorbing areas into carbon sources. Understanding these dynamics is essential for addressing climate change effectively.

This study presents a preliminary analysis of the relationship between SOC and landslide hazard levels across different landslide types in Italy. The overall goal is to provide insights into the complex interplay between landslides, carbon stocks, and the carbon cycle, which is crucial for sustainable land management, hazard mitigation, and climate change adaptation strategies.

2. Materials and Methods

In order to investigate the relation between hazard level and SOC, a landslide susceptibility map is prepared and then it is correlated with the SOC map (Figure 1). The methodology used to build the LSM is explained in Section 2.1. Section 2.2 illustrates the approach used to elaborate the SOC map and obtain the SOC for different hazard classes. Section 2.3 illustrates the methodology used to calculate the changes in AGB and SOC after a landslide event.

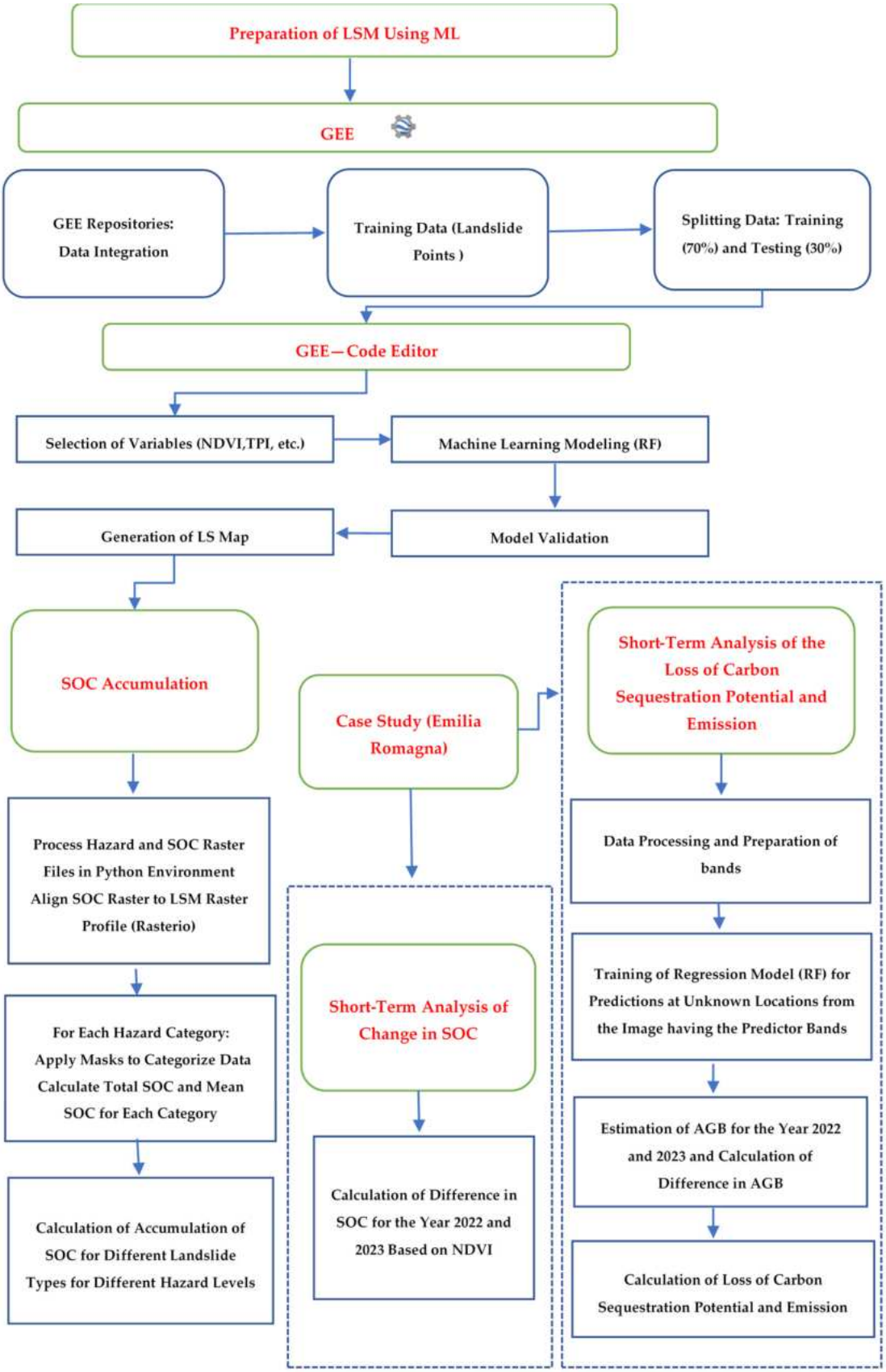

Figure 1. Schematic diagram of LSM framework and specific processing steps for each part (Sections 2.1–2.3).

2.1. Landslide Susceptibility Map

There are different methodologies that can be used to assess landslide susceptibility. In recent years, the use of traditional machine learning methods and deep learning methods has significantly increased and they have been shown to be robust and accurate [51]. The quality of an LS map produced by a model relies heavily on the accuracy, scale, and number of landslide-related factors considered as well as the completeness of the landslide inventory [52]. With the emergence of Google Earth Engine (GEE), there are abundant data resources and functions, which enable investigations at the regional and global scales [53,54].

This study employs the Random Forest (RF) machine learning method to assess landslide susceptibility on a large scale using the Google Earth Engine (GEE) platform at the pixel level [53]. The RF algorithm, renowned for its efficiency in managing high-dimensional datasets, is widely utilized in satellite-based applications due to its computational power and versatility [55]. This model is celebrated for its reliability, ease of interpretation, and robust predictive performance. By constructing multiple decision trees during training, the RF model determines classifications based on the majority vote across these trees. Its resistance to overfitting and multicollinearity makes it an excellent choice for landslide susceptibility assessment, a domain characterized by the interaction of numerous interrelated variables. Furthermore, the RF model provides valuable insights into feature importance, which enhances its interpretability and supports informed decision-making.

For this analysis, the RF model was trained and tested using data from two major landslide inventories: the Italian Landslide Inventory (IFFI) (https://www.progettoiffi.isprambiente.it/en/italian-landslide-inventory-iffi/) and ITALICA (https://doi.org/10.5281/zenodo.8009366) last accessed on 30 July 2024.

The IFFI database is a collaborative initiative led by national, regional, and provincial geological surveys to systematically document landslides across Italy [56]. This extensive inventory includes data on 622,439 landslides, covering a total area of approximately 22,500 km^2, which constitutes about 7.5% of Italy's total land area. The average density of landslides recorded is two per square kilometer. The data within IFFI are derived from diverse sources, including aerial photograph interpretation, analysis of historical records, field surveys, and pre-existing geological maps [56]. The inventory classifies landslides into several types, such as fall and/or topple (26,519 cases), slow (earth) flow (81,513 cases), rapid flow (81,213 cases), complex movement (59,472 cases), rotational/translational slides (222,653 cases), lateral spread (79 cases), sinkholes (409 cases), and undefined slope movements (36,379 cases).

ITALICA is a specialized inventory cataloging 6312 rainfall-triggered landslides that occurred in Italy between January 1996 and December 2021. Unlike the IFFI, ITALICA focuses exclusively on landslides caused by rainfall and provides precise temporal and spatial data. These landslides are evenly distributed across Italy's mountainous and hilly regions. ITALICA is distinctive in its emphasis on temporal accuracy and its exclusive focus on rainfall-induced landslides, setting it apart from IFFI, which covers landslides triggered by various causes but lacks detailed temporal data.

For this study, the two inventories were combined to create a comprehensive dataset for training and validating the RF model. By merging the strengths of both datasets—the IFFI's extensive spatial coverage and ITALICA's precise temporal focus—this approach ensures a robust and well-rounded dataset for landslide susceptibility analysis.

The combined dataset includes nine distinct landslide types (Table 1): slow (SL), complex (C), rotational/translational (RT), shallow (SH), fall (F), rapid (R), diffused fall (DF), Deep-Seated Gravitational Slope Deformations (DSGSDs) from the IFFI and rainfall-triggered (RT) landslides from ITALICA.

This integration offers a holistic view of landslide susceptibility by accounting for a wide variety of factors and types, providing a rich dataset for comprehensive analysis (Tables 2 and 3). In landslide studies, researchers emphasize the variability of factors influencing landslide occurrences across different areas. Identifying relevant causal factors

is challenging, and there is no well-established rule regarding the necessary number of factors for landslide susceptibility analysis. The choice of predisposing factors relies on the unique characteristics of the study area, expert opinions, and the availability of data to generate suitable spatial and thematic patterns [33,57]. In this study, the selected variables for this analysis are listed in Table 2. Aspect, eastness, elevation, Gaussian curvature, HAND (Height Above Nearest Drainage), hillshade, horizontal curvature, maximal curvature, mean curvature, minimal curvature, northness, shape index, slope, TPI (Topographic Position Index), and vertical curvature are derived from a 30 m spatial resolution digital elevation model (DEM) using Google Earth Engine. The Normalized Difference Vegetation Index (NDVI) is derived at a 30 m spatial resolution from Landsat 8 imagery, accessed through the Google Earth Engine (GEE) data catalog. Soil density information, at a 250 m resolution, is sourced from OpenLandMap and accessed through GEE. Additionally, precipitation data from the Global Precipitation Measurement (GPM) Integrated Multi-satellitE Retrievals for GPM (IMERG) product, which provide global rainfall estimates at an 11,132 m resolution, are incorporated. This dataset, provided by NASA GES DISC, is also accessible via GEE. Table 3 summarizes the list of applied datasets and the source.

Table 2. Variables' definitions and rationale used in the model.

Variable	Importance and Rationale	Variable	Importance and Rationale
Aspect	The compass direction that a slope faces. It impacts how much sun exposure the slope receives and the direction of water runoff, influencing the likelihood of landslides. Aspects facing the direction of frequent heavy rains might be more susceptible to landslides.	Mean Curvature	The average of the maximum and minimum curvature of the terrain. It provides an overall indication of the "bendiness" of the terrain, which can impact slope stability and susceptibility to landslides.
Eastness	A sine transformation of the aspect used to handle the circular nature of aspect data. It quantifies the degree to which the slope faces east. Eastern slopes might have different vegetation or water drainage patterns than western slopes, affecting the stability of the slopes.	Minimal Curvature	The minimum amount of curvature in any direction of the terrain. Areas with high minimal curvature might be more prone to landslides due to potentially weaker structural integrity.
Northness	A cosine transformation of the aspect used to handle the circular nature of aspect data. It quantifies the degree to which the slope faces north. Northern slopes might have different vegetation or water drainage patterns than southern slopes, impacting landslide susceptibility.	Vertical Curvature	Measurement of the curvature of the terrain in the vertical plane. This can influence how water flows down a slope, which could impact the saturation of the slope and, consequently, its stability.

Table 2. *Cont.*

Variable	Importance and Rationale	Variable	Importance and Rationale
Elevation	The height of an area above sea level. Higher areas tend to be more prone to landslides due to gravitational forces. Additionally, elevation might impact factors such as temperature and rainfall, which can affect slope stability.	HAND (Height Above Nearest Drainage)	The vertical distance of a location above the nearest water body. Locations closer to water bodies are more susceptible to landslides due to the possible saturation of soil. The greater the HAND, the less likely it is that the area will become saturated and prone to landslides.
Gaussian Curvature	A measure of the total curvature of the terrain. This is calculated as the product of the maximal and minimal curvature of the terrain. Extreme positive or negative Gaussian curvature can suggest that the terrain is convex or concave, respectively, which can influence water runoff and slope stability.	Hillshade	A measure that indicates the amount of sunlight a region receives. Regions receiving more sunlight might have lower soil moisture levels and different vegetation types compared to those receiving less sunlight. These factors can impact slope stability and susceptibility to landslides.
Horizontal Curvature	Measurement of the curvature of the terrain in the horizontal plane, potentially affecting the direction and speed of water flow. A high horizontal curvature might lead to faster water flow, possibly accelerating soil erosion and increasing landslide susceptibility.	Shape Index	Quantification of the shape of the terrain, giving an idea of landscape relief. This can help identify areas of potential water pooling or steep gradients, both of which can impact landslide occurrence. High shape index values typically correspond to ridges and peaks, while low values represent valleys and depressions.
Maximal Curvature	Reflection of the maximum amount of curvature in any direction of the terrain. Regions with high maximal curvature might be more prone to landslides due to potentially weaker structural integrity.	Rain (Mean Precipitation)	Mean monthly precipitation from IMERG GPM. The data were resampled to 30 m for landslide susceptibility model training.
TPI (Topographic Position Index)	A measure that indicates the position of an area in relation to its surroundings (e.g., valley, ridge, flat area). It helps understand the influence of landscape position on the direction and speed of water flow, which can affect soil saturation levels and landslide susceptibility.	Slope	The angle of the terrain, or steepness. Steeper slopes are generally more susceptible to landslides as the unstabilizing component of the gravitational force acting on the slope material is greater.
NDVI	NDVI is an indicator of Vegetation Health Assessment, Stability Indicator, and Rainfall and Erosion Control. High NDVI values indicate healthy vegetation, while low values suggest sparse or stressed vegetation.	Soil Density	Soil density may influence shear strength, water retention properties, and erosion susceptibility.

Table 3. Data sources utilized in the study.

Data	Resolution	Source	URL
NDVI (Normalized Difference Vegetation Index)	30 m	Google Earth Engine	https://developers.google.com/earth-engine/datasets/catalog/landsat-8, last accessed on 30 July 2024
NASA SRTM Digital Elevation 30 m	30 m	Google Earth Engine	https://developers.google.com/earth-engine/datasets/catalog/USGS_SRTMGL1_003#description, last accessed on 30 July 2024
Spatio-Temporal Catalog of Rainfall-Induced Landslides in Italy		ITALICA	https://doi.org/10.5281/zenodo.8009366, last accessed on 30 July 2024
Soil Density	250 m	Google Earth Engine	https://developers.google.com/earth-engine/datasets/catalog/OpenLandMap_SOL_SOL_BULKDENS-FINEEARTH_USDA-4A1H_M_v02#description, last accessed on 30 July 2024
Landslide Inventory in Italy		IFFI catalog	https://www.progettoiffi.isprambiente.it/en/italian-landslide-inventory-iffi/, last accessed on 30 July 2024
Rainfall (Precipitation)	11,132 m	Google Earth Engine	https://disc.gsfc.nasa.gov/datasets/GPM_3IMERGM_07/summary, last accessed on 30 July 2024
SOC	250 m	Google Earth Engine	https://developers.google.com/earth-engine/datasets/catalog/OpenLandMap_SOL_SOL_ORGANIC-CARBON_USDA-6A1C_M_v02, last accessed on 15 October 2024

The landslide inventory is split into two sets: 70% for training and 30% for testing. The Random Forest model was trained on the 70% subset, optimized for minimum out-of-bag error, and the final model was selected based on this optimization. The final model, optimized through training on the 70% dataset, was employed to predict landslide susceptibility for the remaining 30% testing data subset. These predictions were then compared with actual values, and the accuracy of the model was assessed using the AUC-ROC (Area Under the Receiver Operating Characteristic) method. Subsequently, the chosen model was applied to the entire geographic extent of Italy. The outcome was a probability-based landslide susceptibility map, ranging from 0 to 100. This map was further classified into 6 classes indicating landslide susceptibility scores based on their likelihood of experiencing landslides: very low (0–15%), low (15–30%), low to moderate (30–45%), moderate to high (45–60%), high (60–80%), and very high susceptibility (80% and above). Different maps are prepared for each type of landslide (Figure 2a,b).

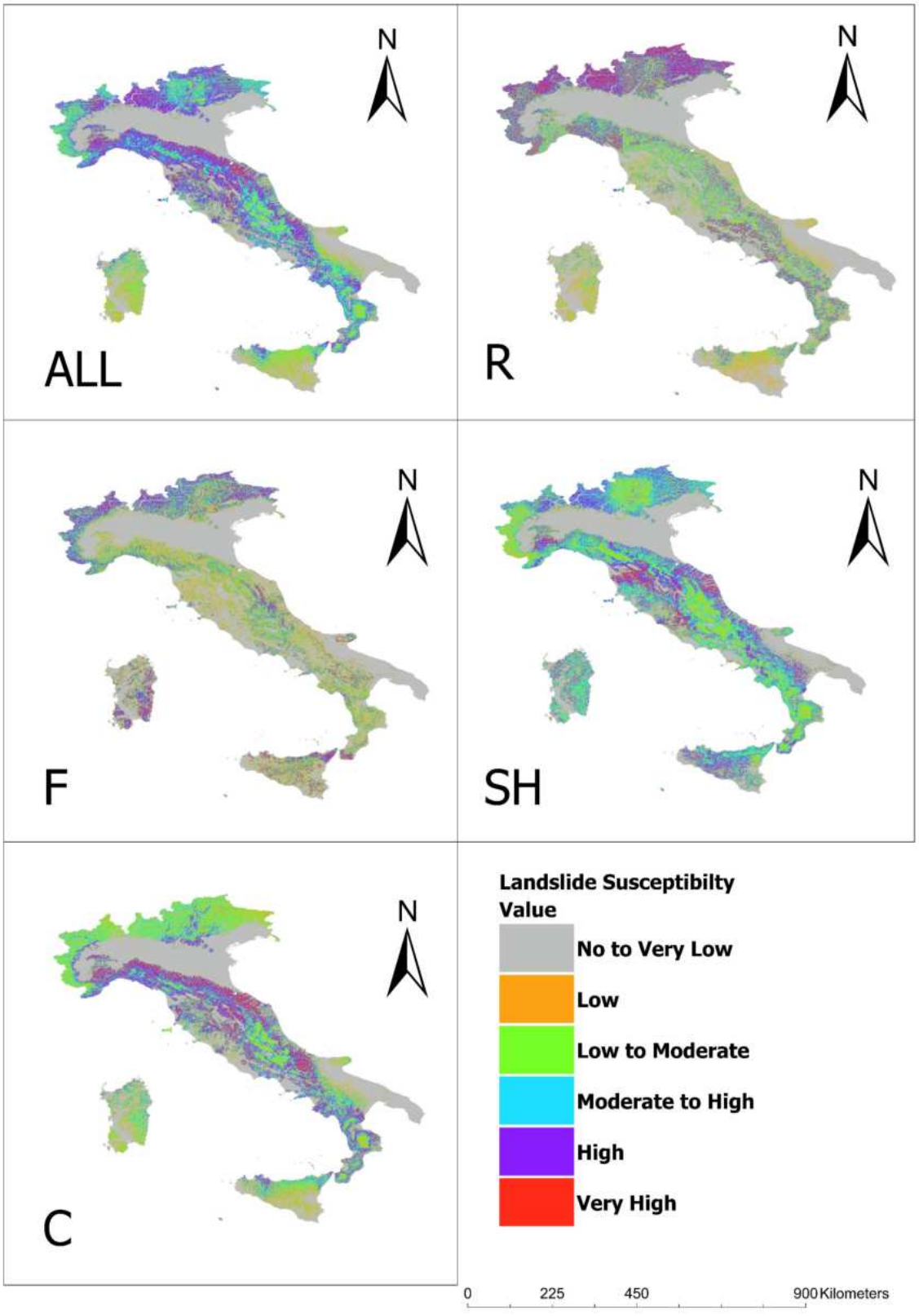

(**a**)

Figure 2. *Cont*.

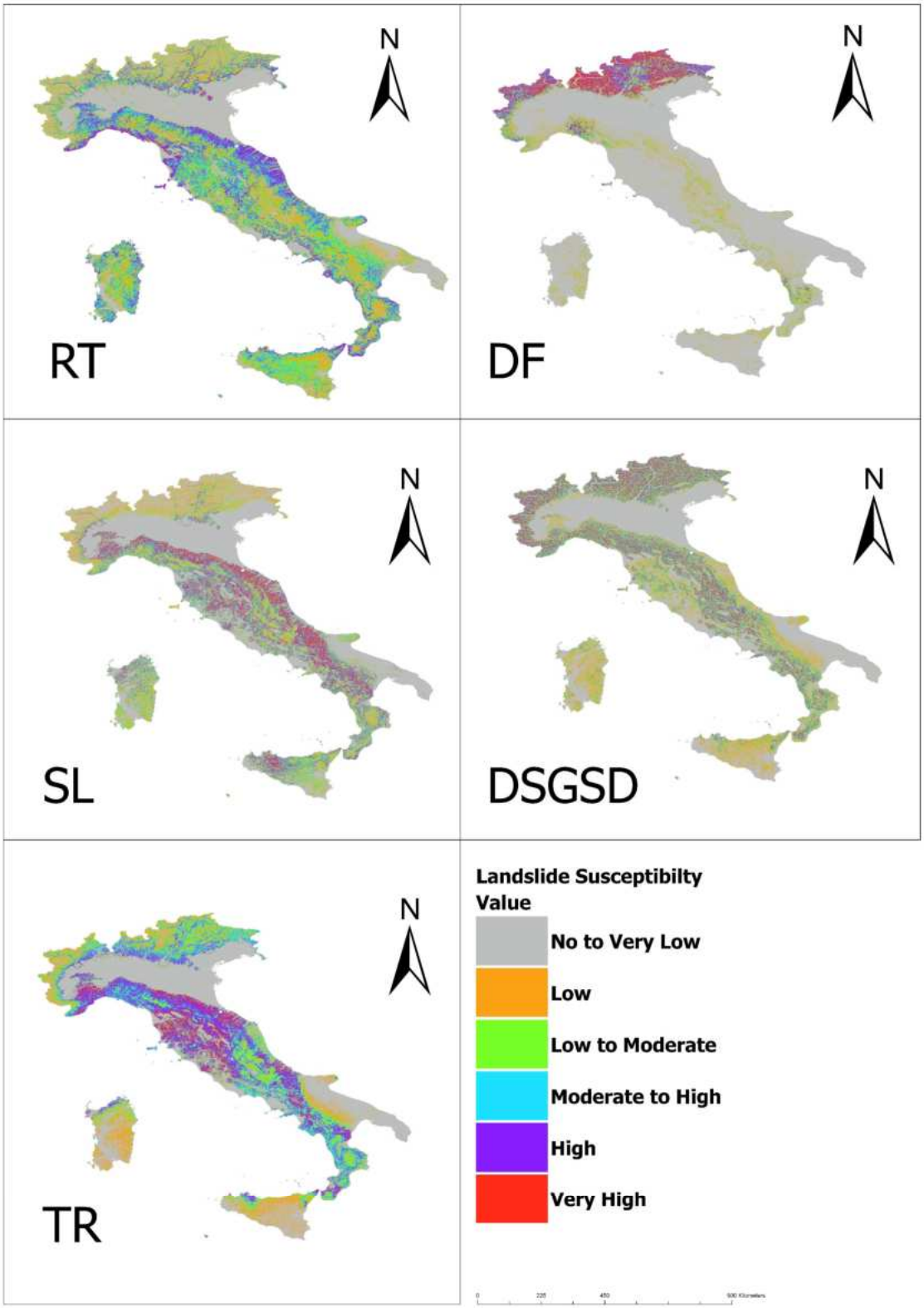

(**b**)

Figure 2. (**a**) Landslide susceptibility map for all, R, F, SH, and C landslide types. (**b**) Landslide susceptibility map for RT, DF, SL, DSGSD, and TR landslide type.

2.2. SOC and Hazard Categories

The map of SOC is taken from OpenLandMap available on GEE, and it represents soil organic carbon content in $\times 5$ g/kg at 6 standard depths (0, 10, 30, 60, 100, and 200 cm) at a 250 m resolution. The algorithm processes different landslide hazard maps and SOC raster files in a Python environment to compute and visualize SOC values for different hazard categories. It aligns the SOC raster to the hazard raster profile using the rasterio library and calculates total and average SOC values for predefined hazard categories.

The primary function in the Python environment serves multiple purposes in analyzing the relationship between hazard levels and soil organic carbon (SOC). It begins by reading the input hazard raster and SOC raster files, which contain spatial data on hazard levels and soil organic carbon content, respectively. The function then applies masks to categorize the data based on predefined hazard levels. This categorization enables a detailed examination of how SOC is distributed across areas with varying hazard intensities.

Then, the function aggregates SOC values within each hazard category to calculate total soil organic carbon (total SOC) and mean soil organic carbon. Total SOC represents the cumulative sum of SOC across all soil areas within the specified hazard category while mean SOC is the average SOC value for the areas within each hazard category, providing a normalized measure of SOC distribution.

Finally, the function visualizes the results by plotting the total and mean SOC values, offering clear insights into the relationship between hazard levels and SOC distribution. This analysis highlights how soil organic carbon varies across different hazard intensities, aiding in understanding the interplay between environmental hazards and soil health.

Total SOC is typically expressed in mass units such as megagrams (Mg) or tons. Mean soil organic carbon is the average organic carbon content per unit area in the soil. It represents the concentration of soil organic carbon averaged across a specified area. It is typically expressed in mass per area units such as megagrams per hectare (Mg/ha) or tons per hectare (tons/ha) for each category and saves the plots for further analysis.

2.3. Above-Ground Biomass Density (AGBD) Calculation and Change in SOC

This section considers the case of the intense rainfall events that occurred in May 2023 in Emilia Romagna (Italy) causing more than 60 thousand landslides of different types (See Section 3.3). All landslide polygons are mapped including the source and deposition area (https://geoportale.regione.emilia-romagna.it/approfondimenti/emergenza-maggio-23/emergenza-rer-maggio-2023-servizi, accessed on 15 December 2024).

Two distinct methodological approaches are employed to quantify the impact of landslides on carbon stocks in the Emilia Romagna landslide-affected region:

1. The first method utilizes remote sensing data to find the change in SOC based on the Normalized Difference Vegetation Index (NDVI).
2. The second method leverages data from NASA's Global Ecosystem Dynamics Investigation (GEDI) mission to calculate AGB density. GEDI's lidar measurements, combined with Sentinel-2 satellite data and elevation models, are used to train a regression model for predicting AGB density.

Methodology (1) first defines pre- and post-landslide time periods and filters the Landsat collection to include only images with less than 20% cloud cover over the Emilia Romagna, then calculates NDVI for both periods, masks invalid NDVI values, and converts the NDVI to SOC and carbon stock estimates. The change in carbon sequestration is calculated by finding the difference between pre- and post-landslide carbon stocks.

Method (2) tries to quantify the loss in AGB. To evaluate and quantify the density and total stock of above-ground biomass, we selected only the landslide polygons out of the whole of Emilia Romagna with the aim of finding the difference between 2022 and 2023. We used GEDI mission data utilizing the MIT open-source data and adapted them according to our requirements. NASA's GEDI mission collects LIDAR measurements at a 30 m spatial resolution, capturing the vertical distribution of vegetation to estimate above-ground biomass density (AGBD) [58]. These point estimates serve as ground-truth data for

regression models. The present study utilizes Sentinel-2 satellite data, including spectral bands and indices, which are cloud-masked using Google's Cloud Score dataset to create an annual cloud-free composite. Elevation and slope data from the Copernicus GLO-30 DEM are incorporated both for pre-processing GEDI data and as independent variables. Data preparation involves filtering, scaling, and creating mosaics for each dataset. GEDI data are filtered to remove unreliable measurements based on quality flags, relative error, and slope constraints, while Sentinel-2 images are processed to a median composite. Thereafter, all datasets are exported as assets to manage computational limitations.

In building the regression model, Sentinel-2 data, along with elevation and slope, are used as predictors, while GEDI AGBD values serve as the target variable. Resampling and stratified sampling techniques ensure alignment and adequate coverage of valid data points. The trained regression model predicts AGBD values, which are then used to estimate total AGB [59]. To refine this estimation, non-vegetated pixels are masked using the ESA World Cover dataset, and the total AGB is calculated by multiplying the AGBD values by each pixel's area and summing them across the region for both years (2022 and 2023), and the whole process is carried out on the GEE platform.

This model is then applied to the study area and the total AGB is quantified by integrating the AGBD values over the landslide-affected regions (polygons). By comparing the AGB estimates before and after the landslide event, the impact on above-ground carbon stocks can be assessed. The total AGB is calculated for the landslide area (polygons) by multiplying the AGBD values by each pixel's area under the landslide polygons and summing them across the landslide polygon regions for 2022 and 2023.

3. Results

This section illustrates and comments on the results first in terms of landslide susceptibility maps and then as SOC for each landslide hazard class.

3.1. Landslide Susceptibility Map

The landslide susceptibility maps obtained from the RF model introduced in the previous section are shown in Figure 2a,b, and the area falling in each susceptibility class for each type of landslide is summarized in Table 4 and graphically represented in Figure 3. The category "All" considers all types of landslides together without any specific distinction. A better-quality map can be downloaded.

Table 4. Areas (km^2) susceptible to different classifications of landslide types obtained from landslide susceptibility maps.

Landslide Type	Very Low	Low	Low to Moderate	Moderate to High	High	Very High
All	108,946.32	21,889.13	37,932.82	50,740.72	59,646.97	21,234.00
C	114,908.24	29,582.67	49,590.01	42,575.07	38,765.48	24,968.48
R	142,295.21	38,029.22	32,718.32	30,164.43	32,311.75	24,871.02
SH	97,312.387	23,854.49	49,941.89	62,858.51	46,691.48	19,731.20
F	139,696.10	45,507.46	34,386.96	28,975.88	28,991.85	22,831.71
TR	115,278.79	37,629.80	35,121.60	38,506.51	47,503.96	26,349.30
RT	81,825.44	53,948.82	56,061.36	49,942.25	39,319.29	19,292.79
DSGSD	141,084.88	51,165.93	34,987.85	24,515.30	24,594.20	24,041.80
SL	143,512.69	42,859.43	32,029.03	25,190.49	27,897.97	28,900.35
DF	212,932.59	25,752.76	13,077.50	9198.00	12,480.37	26,948.74

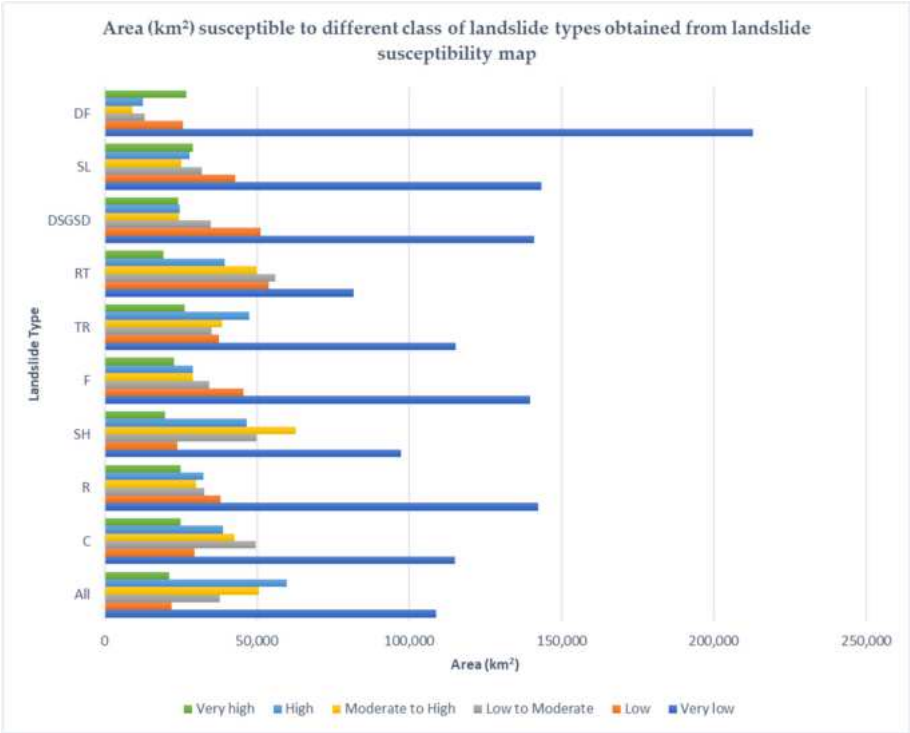

Figure 3. Areas (km^2) susceptible to different classifications of landslide types obtained from landslide susceptibility maps.

The model performances were evaluated using the Area Under the Receiver Operating Characteristic Curve (AUC-ROC), a metric that measures a model's ability to correctly distinguish between landslide and non-landslide areas (Figure 4). Specifically, the ROC curve plots the true positive rate (sensitivity) against the false positive rate (1 − specificity) at various classification thresholds. The area under this curve represents the model's ability to distinguish between positive (e.g., landslide) and negative (non-landslide) instances. An AUC-ROC score of 1 represents a perfect model, while a score of 0.5 implies performance no better than random chance. Generally, the higher the AUC-ROC value, the better the model's performance in separating the two classes. The models in this study achieved AUC scores ranging from 0.84 to 0.96, as shown in Figure 4, indicating strong overall accuracy and reliable predictions. Overall, higher AUC values reflect stronger model performance, with curves farther from the diagonal line indicating more accurate classification. Although not flawless, these scores suggest that the models are robust enough for assessing landslide susceptibility, effectively differentiating between areas at risk and those that are not.

Among the different landslide types, the model for diffused fall (DF) performed best with an AUC of 0.96, demonstrating excellent predictive power. The slow landslide classifier followed closely with an AUC of 0.91, reflecting strong accuracy, while the complex landslide model scored 0.87, indicating good but slightly lower performance. Other landslide types, such as rainfall-triggered (RT) and shallow landslides (SH), had AUC values of 0.85 and 0.84, respectively, indicating decent accuracy. The models for Deep-Seated Gravitational Slope Deformations (DSGSDs) and rapid landslides also performed well, both achieving AUC values between 0.91 and 0.92. The TR landslide model had an AUC of 0.86, indicating reasonable but improvable performance.

By this methodology, it is also possible to investigate variable importance (Figure 5); among the variables, rain and NDVI have the highest importance, followed by elevation in the case of all landslide types. HAND, slope, hillshade, soil density, and curvature metrics are moderately important. These are essential but not as critical as rain and NDVI. Variables like minimal curvature, shape index, and aspect have the least importance but still contribute to the model, while in the case of rainfall-triggered landslides (RT), elevation,

NDVI, and rain are the most important. It seems that when rain is explicitly modeled, elevation becomes significantly more critical, surpassing rain itself. This is because intense rainfall is the triggering factor of these mass movements, but the variable rainfall in the model represents a major causative factor and it is understood as a predisposing factor. Soil density, HAND, and slope follow, with hillshade and northness being slightly less important. Variables related to curvature and orientation (like curvature and aspect) have a lower influence.

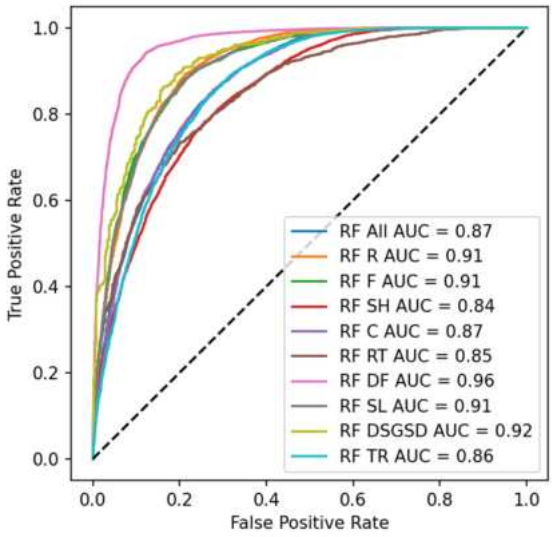

Figure 4. AUC-ROC for all, R, F, SH, C, RT, DF, SL, DSGSD, and TR landslide types.

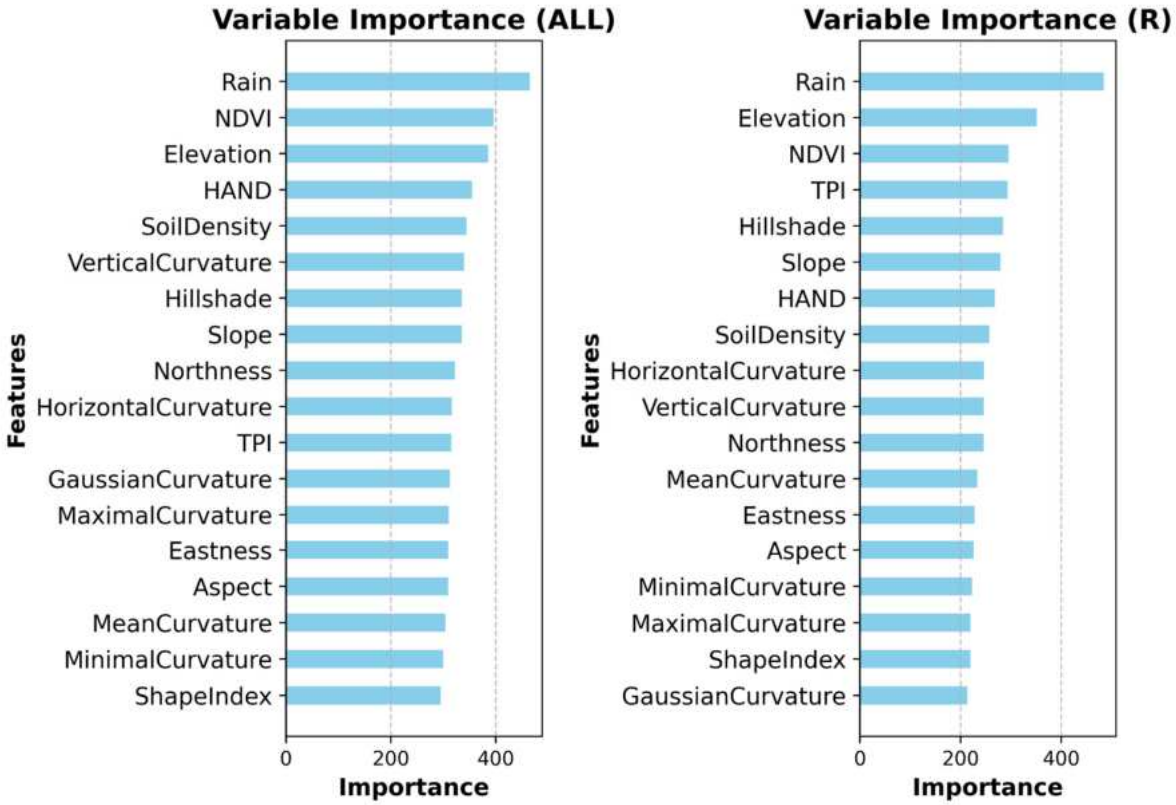

Figure 5. *Cont.*

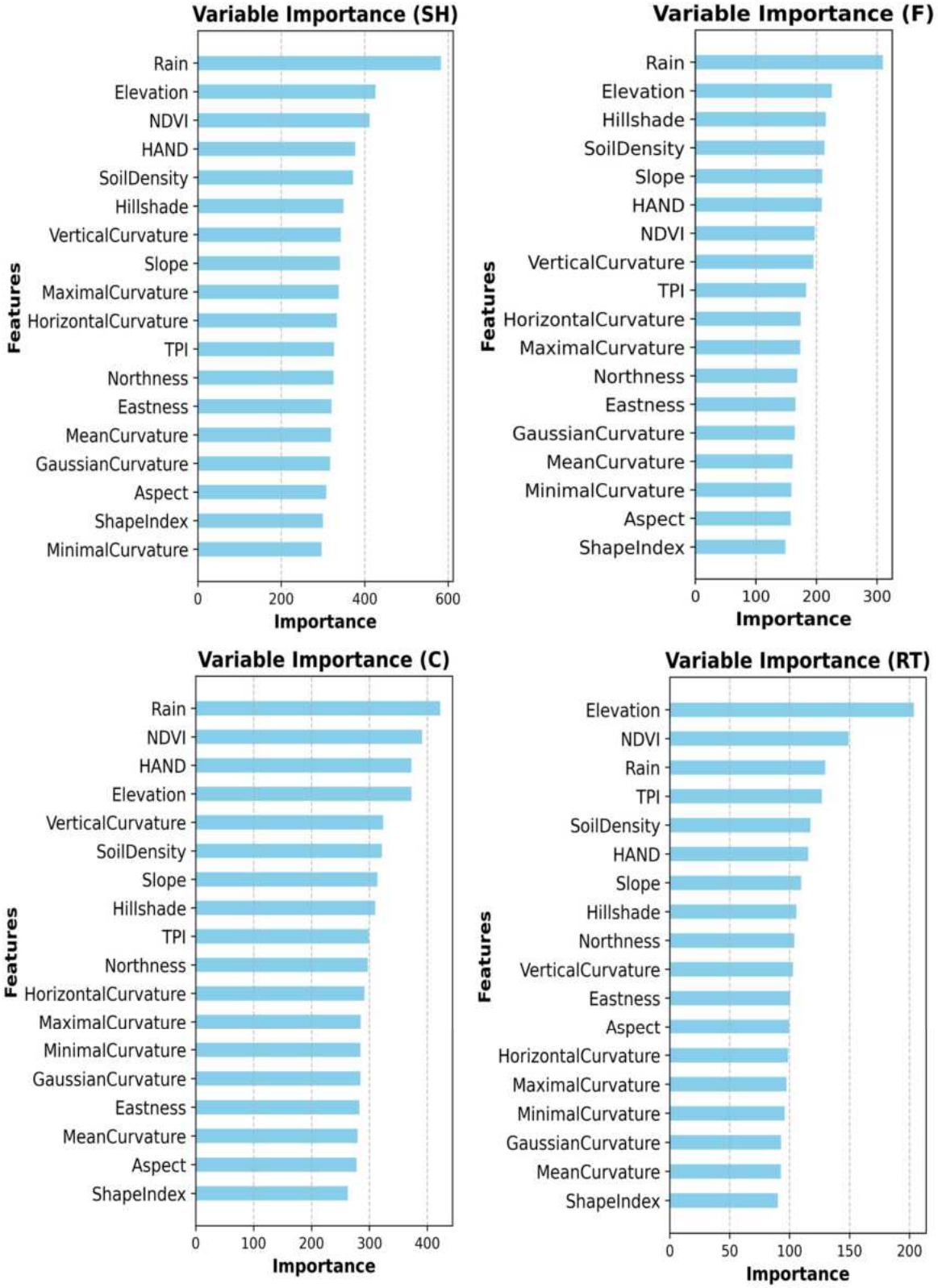

Figure 5. *Cont*.

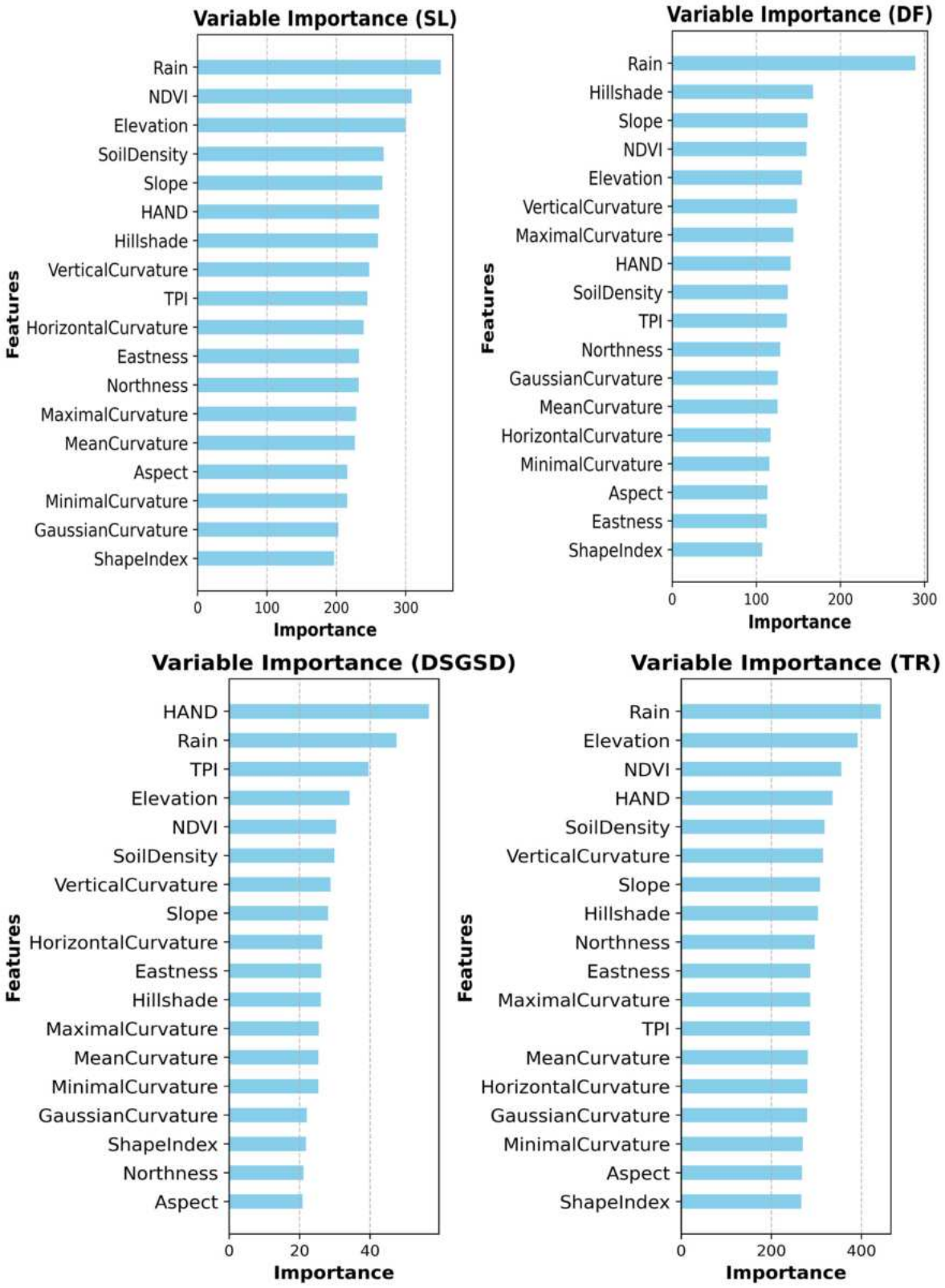

Figure 5. Feature importance for all, R, F, SH, C, RT, DF, SL, DSGSD, and TR landslide types.

In the case of the landslide type fall (F), rain dominates in importance, as comparable to other models. This suggests that rain is the most influential factor, which may be due to the weathering effect of rock slopes. Elevation and hillshade follow as the next most important. Soil density, HAND, and slope are important but significantly less than rain

and elevation. Features like maximal curvature, northness, and eastness have relatively low importance. In the case of DSGSDs, HAND and rain are the most critical variables; TPI and elevation follow in importance but are significantly less impactful than HAND and rain. NDVI, soil density, and vertical curvature are moderately important but not as critical as the top features. Variables like northness, aspect, and shape index also have a significant impact.

We can draw an inference that each model gives a unique perspective on how environmental factors like terrain and climate variables influence outcomes. Rain is the most critical driver of landslide risk in most models, emphasizing that precipitation is not only a primary trigger for landslide events but also an important predisposing factor. High elevations and steep slopes consistently rank as important factors due to their impact on slope stability. Vegetation (NDVI) helps reduce landslide risk by stabilizing the soil, making this an essential factor in most models. Proximity to drainage networks is vital in landslide susceptibility (HAND), likely due to water's role in destabilizing slopes. Features like curvature, aspect, and TPI are less critical than rainfall and elevation but still influence landslide patterns by affecting runoff and erosion dynamics. Soil density and hillshade reflect soil properties and sunlight exposure, which indirectly impact landslide susceptibility. Each model gives the importance of variables based on seasonal or dynamic factors, reflecting how different environmental conditions influence landslide risk in various contexts.

3.2. SOC and Landslide Hazard Class

Figure 6 shows the total SOC and the mean SOC per unit of area in each landslide susceptibility class. Each subplot corresponds to a specific landslide type, and the x-axis represents the hazard level (ranging from 0 to 4), while the y-axis displays the total SOC (blue bars) and mean SOC (red line). Overall, this figure highlights the varying spatial relationships between SOC accumulation and landslide hazard levels across different landslide types. Some types, such as complex, shallow, rotational, and slow landslides, exhibit a decreasing trend in SOC with increasing hazard levels in classes 1 to 4; this may suggest that there is a beneficial effect of SOC in landslide hazard, but also that landslides that occurred in the past in highly susceptible areas had a negative effect of SOC. Other types of landslides, such as F, R DSGSD, and DF landslides, show an increasing trend. The elevated presence of SOC in highly susceptible areas may indicate that there are factors that increase both SOC and landslide hazards. For example, areas with high SOC often coincide with topographic features and climatic conditions that are inherently more susceptible to landslides, such as steep slopes, convergent topography where organic matter accumulates, or wet areas.

Considering all types of landslides together, low hazard levels (0 and 1) show limited mean and total SOC because these are typically urbanized and agricultural areas. Decreasing levels of mean and total SOC are observed for higher hazard levels (2 to 4), probably indicating that this factor may contribute positively to landslide hazard. At the same time, it is possible to observe that there is a significant amount of carbon stored in high or very high susceptibility classes which may become a carbon source if a landslide occurs.

These patterns suggest that the influence of landslides on SOC dynamics may vary depending on the specific landslide type and the environmental conditions associated with each type. Indeed, SOC is influenced by different factors, such as soil type, slope angle, rainfall patterns, and underlying geology, some of which are also relevant for landslide susceptibility, but in different measures depending on the landslide type. This can be useful for future studies related to soil health, carbon sequestration, and ecological balance. The interpretation provided and discussed in the present study should be regarded as a preliminary observation. While it offers initial insights, it requires further validation to ensure its accuracy and reliability. This can be achieved through additional field data collection, controlled experiments, or further supplementary studies. Such validation steps are essential to confirm the findings and strengthen the conclusions drawn from this study.

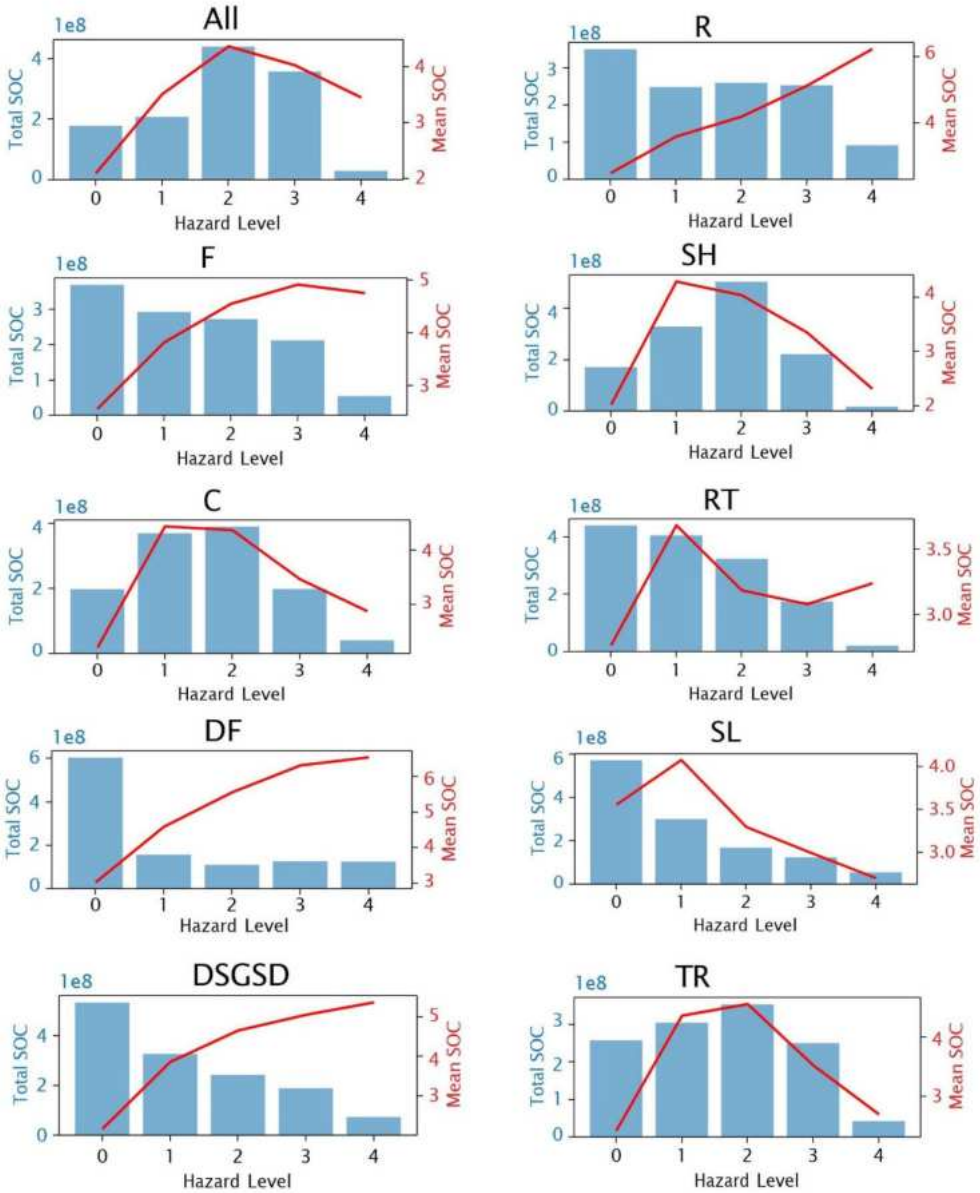

Figure 6. SOC accumulation trends and landslide type hazard level for all, R, F, SH, C, RT, DF, SL, DSGSD, and TR landslide types.

3.3. Short-Term Impact of Landslides on Carbon Stocks

The purpose of this section is to evaluate the impact of landslide events on carbon stocks, specifically soil organic carbon and above-ground biomass (AGB) in the study area (Figure 7). AGB, including leaves, stems, and branches, contributes to soil organic carbon through the addition of organic matter from litterfall, plant decomposition, and root exudates. Larger above-ground biomass often indicates a more extensive root system, which directly adds organic matter to the soil and supports microbial communities that decompose plant material into stable SOC forms. This biomass is crucial for carbon sequestration, as healthy vegetation captures atmospheric CO_2 and stores it in plant tissues, thus enhancing carbon storage in both the plant and soil. Changes in AGB can significantly impact SOC, influencing soil health, structure, fertility, and overall ecosystem productivity. Positive feedback loops can enhance biomass and SOC, improving soil conditions and promoting further growth, while negative feedback loops can degrade soil and reduce plant growth. Understanding the effects of landslides on these crucial carbon reservoirs is

essential for assessing the overall influence on the carbon cycle and potential implications for climate change.

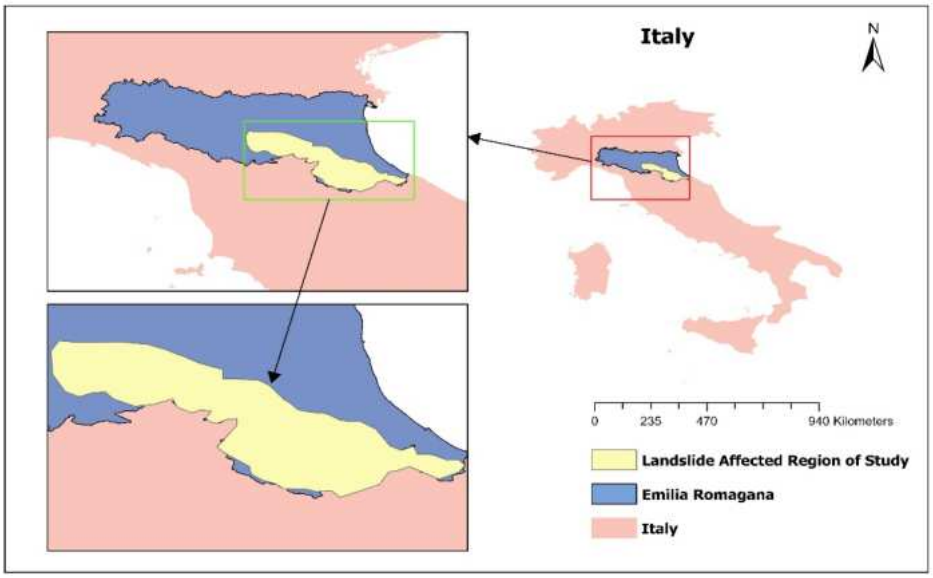

Figure 7. Landslide-affected region.

The analysis of SOC changes based on NDVI revealed that a larger area (approximately 21 million square meters) (Figure 8) experienced a decrease in SOC accumulation. However, a smaller area (around 8 million square meters) exhibited an increase in SOC, potentially due to environmental recovery or ecosystem shifts following the landslide event. In Figure 8, the red areas show negative carbon stock change, and the blue areas show positive carbon stock change. Negative sequestration change indicates a reduction in the area's ability to capture and store carbon. Positive sequestration change means that in this part of the landslide-affected area, there has been an increase in the ability to sequester carbon.

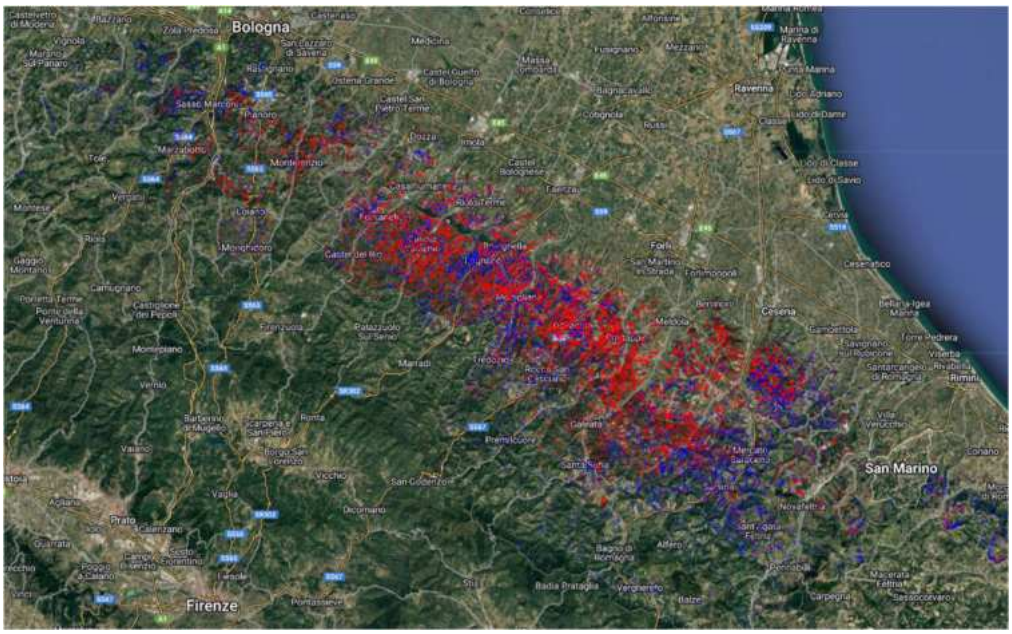

Figure 8. Impact of landslides on vegetation and carbon sequestration by comparing the NDVI (Normalized Difference Vegetation Index) and biomass levels before and after the landslides in the region.

To evaluate and quantify the density and total stock of above-ground biomass, we selected only the landslide polygons out of the whole of Emilia Romagna with the aim of finding the difference between 2022 and 2023. By comparing the AGB estimates before and after the landslide event, the impact on above-ground carbon stocks can be assessed. Figure 9 shows the AGBD difference before and after the event of the entire affected area.

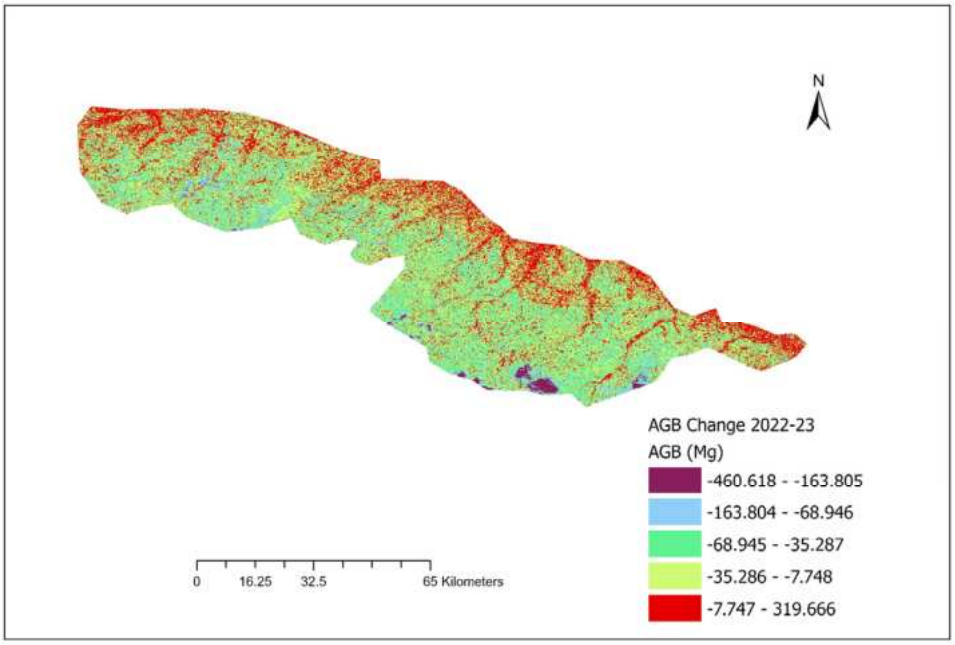

Figure 9. Above-ground biomass density difference between 2022 and 2023.

The comparison of AGB estimates before and after the landslide event showed a significant decrease in above-ground biomass, from 750,266.23 Mg in 2022 to 484,902.34 Mg in 2023. This reduction in AGB suggests that less carbon is being stored in the above-ground vegetation, potentially leading to the release of previously sequestered carbon into the atmosphere.

The loss of 265,364 Mg (megagrams) of AGB may lead to the release of 487,000 metric tons of CO_2 (see Appendix A), which could contribute to atmospheric greenhouse gases, exacerbating climate change. This is a significant loss of carbon sequestration potential from landslide-affected areas, contributing to the local and regional environmental imbalance.

4. Discussion

This section discusses the findings of this study in the context of the existing literature, highlights its limitations, and explores its implications for understanding the interplay between landslides, soil organic carbon (SOC), and the carbon cycle.

The analysis presented in Section 3.2 investigated, for the first time in the literature, patterns between landslide hazard levels and SOC accumulation. The results reveal that the trends depend on the landslide types. The overall trend indicates a decrease in SOC stocks with increasing landslide susceptibility, suggesting a correlation between environmental conditions and SOC accumulation, with higher susceptibility areas potentially experiencing lower SOC levels. This suggests that, on one hand, SOC may be beneficial for landslide hazard reduction, and on the other hand, there is a significant amount of SOC stored in highly susceptible areas, which may potentially become a source of CO_2 emission if a landslide occurs.

The results presented in Section 3.3 align with previous research by Cox et al. (2024) [29] and Frith et al. (2018) [30], which examined carbon losses associated with earthquake-induced landslides. Cox et al. [29] reported total carbon losses of 2.05 Mt and 0.217 Mt from major events in New Zealand, indicating significant short-term carbon disruptions relative to the region's annual carbon sequestration (6.3 Mt in 2020). Similarly,

Frith's simulations estimated a potential erosion of 14 ± 5 MtC from a single large earthquake. In contrast, the current study focused on rainfall-triggered landslides in Emilia Romagna and observed a loss of 265,364 Mg of above-ground biomass (AGB), equivalent to 0.133 MtC. While these losses are smaller in magnitude, it should be noted that our study is focused on the landslide polygons and not on the scale of the region as was examined in previous studies. This underscores the localized but significant impact of rainfall-triggered landslides on carbon dynamics.

Unlike earthquake-induced events, which are less frequent, rainfall-triggered landslides are expected to increase in frequency due to climate change. This cumulative effect represents a substantial risk to regional carbon storage, emphasizing the importance of rainfall-triggered events in long-term carbon assessments. The observed decrease in AGB, a proxy for carbon sequestration, further supports the conclusion that landslides disrupt above-ground carbon stocks and alter the balance between carbon storage and emissions.

The study also highlights the importance of considering recovery timelines, as vegetation regrowth and carbon stock restoration can span decades, influencing long-term carbon dynamics. Prior studies on post-landslide ecosystem recovery corroborate this finding, indicating that ecosystem resilience plays a critical role in mitigating the carbon impacts of landslides.

While this research provides valuable insights into the spatial relationship between landslides, soil organic carbon (SOC), and the carbon cycle, it is important to acknowledge the following limitations. The findings presented are based on remote sensing data and modeling techniques, which, while powerful, have inherent limitations. The results are preliminary and require further validation through field data collection and experimental studies to confirm the observed patterns and trends. This study focused on specific variables, such as SOC, above-ground biomass (AGB), and landslide susceptibility. However, additional environmental factors, including vegetation diversity, soil moisture, and land-use changes, were not incorporated, which might influence the observed relationships. The study has temporal constraints because the analysis centers on the May 2023 landslide event, providing a snapshot rather than a long-term perspective, which could reveal more about the resilience of ecosystems and carbon dynamics over time. Additionally, the spatial resolution may not fully capture small-scale heterogeneities in SOC dynamics. The estimation of carbon losses, especially CO_2 emissions, is based on established conversion factors and assumptions. These estimates could benefit from direct measurement and validation in affected areas to refine accuracy. The study's findings are based on landslides in Italy, particularly Emilia Romagna, which may limit the generalizability of the conclusions to other regions with different climatic, geological, and ecological conditions.

Future studies should address these limitations by incorporating field data, expanding variable selection, and examining long-term impacts to provide a more comprehensive understanding of landslide–carbon interactions.

5. Conclusions

This study contributes to advancing the current understanding of the relationship between different types of landslides, soil organic carbon (SOC), and the carbon cycle. This relationship has important implications for environmental sustainability and climate change mitigation efforts.

The analysis reveals a pattern between landslide hazard levels and SOC accumulation, with varying trends observed for different landslide types. The overall trend indicates a decrease in SOC stocks with increasing landslide susceptibility, suggesting a correlation between environmental conditions and SOC accumulation. This suggests that SOC may be beneficial for landslide hazard reduction, but there is also a significant amount of SOC in highly susceptible areas, which may potentially become a source of CO_2 emissions if landslides occur.

The case study of the May 2023 landslide event in the Emilia Romagna region of Italy highlights the potential impact of large-scale landslides on carbon sequestration. The

observed decrease in SOC accumulation and AGB in the affected regions indicates that landslides can transform carbon sinks into carbon sources, at least in the short term. The result is a significant loss of carbon sequestration potential in Emilia Romagna and suggests that the effects of landslide events need to be accounted for in regional or national carbon emissions. This phenomenon is particularly concerning as climate change is expected to increase the frequency and intensity of extreme weather events, potentially triggering more landslides and exacerbating the release of stored carbon.

This study underscores the importance of considering landslides in carbon cycle assessments, especially as climate change is expected to induce more extreme weather events, potentially turning carbon-absorbing areas into carbon sources as these extreme events largely contribute to worsening the impacts of climate change. This creates a feedback loop where landslides amplify the climate changes that cause them and lead to environmental imbalance, severe disruptions to biodiversity, soil health, and local climate regulation, with wide-reaching consequences.

This study represents a preliminary step in quantifying the impact of landslides on carbon stocks, utilizing remote sensing data and modeling techniques. While the study provides valuable insights, the authors acknowledge that the interpretations presented are preliminary and require further validation through field data collection, experimental studies, and the incorporation of additional environmental parameters. Further research is necessary to fully understand the interactions between landslides, SOC dynamics, and the carbon cycle. This knowledge is crucial for improving hazard management, developing effective climate change mitigation strategies, and implementing soil conservation measures.

Author Contributions: Conceptualization, J.Q. and F.C.; methodology, J.Q. and F.C.; software, J.Q.; validation, J.Q.; writing—original draft preparation, J.Q. and F.C.; writing—review and editing, J.Q. and F.C.; visualization, J.Q. and F.C.; supervision, F.C.; funding acquisition, F.C. All authors have read and agreed to the published version of the manuscript.

Funding: This study was funded by the European Union—NextGenerationEU, Mission 4, Component 2, in the framework of the GRINS—Growing Resilient, INclusive and Sustainable project (GRINS PE00000018—(GRINS PE00000018—CUP C93C22005270001)). The views and opinions expressed are solely those of the authors and do not necessarily reflect those of the European Union, nor can the European Union be held responsible for them.

Institutional Review Board Statement: Not applicable.

Informed Consent Statement: Not applicable.

Data Availability Statement: The original contributions presented in the study are included in the article, further inquiries can be directed to the corresponding author.

Conflicts of Interest: The authors declare no conflicts of interest.

Appendix A

This appendix illustrates how the amount of carbon dioxide (CO_2) released from the loss of AGB can be estimated. AGB, which refers to plant materials like trees and vegetation, contains around 50% carbon by dry weight [60]. In the considered area, the total AGB loss is 265,364 metric tons; to find the carbon content, we multiply the biomass amount by 0.5 (50%), which gives us 132,682 metric tons of carbon. Since burning biomass releases CO_2, we need to convert the carbon amount to CO_2. This is achieved by multiplying the carbon amount by the ratio of the molecular weights of CO_2 and carbon (44/12 or 3.67). The result is 486,941 metric tons of CO_2 released.

References

1. Yi, C.; Ricciuto, D.; Li, R.; Wolbeck, J.; Xu, X.; Nilsson, M.; Aires, L.; Albertson, J.D.; Ammann, C.; Arain, M.A.; et al. Climate control of terrestrial carbon exchange across biomes and continents. *Environ. Res. Lett.* **2010**, *5*, 034007. [CrossRef]
2. Shiels, A.B.; Walker, L.R.; Thompson, D.B. Organic matter inputs create variable resource patches on Puerto Rican landslides. *Plant Ecol.* **2006**, *184*, 223–236. [CrossRef]
3. Shiels, A.B.; Walker, L.R. Landslides cause spatial and temporal gradients of multiple scales in the Laquillo Mountains of Puerto Rico. *Ecol. Bull.* **2013**, *54*, 211–221.
4. Lopes, L.F.; Oliveira, S.C.; Neto, C.; Zezere, J.L. Vegetation Evolution by Ecological Succession as a Potential Bioindicator of Landslides Relative Age in Southwestern Mediterranean Region. *Nat. Hazards* **2020**, *103*, 599–622. [CrossRef]
5. Gorham, E. Northern Peatlands: Role in the Carbon Cycle and Probable Responses to Climatic Warming. *Ecol. Appl.* **1991**, *1*, 182–195. [CrossRef]
6. Freeman, C.; Fenner, N.; Ostle, N.J.; Kang, H.; Dowrick, D.J.; Reynolds, B.; Lock, M.A.; Sleep, D.; Hughes, S.; Hudson, J. Export of dissolved organic carbon from peatlands under elevated carbon dioxide levels. *Nature* **2004**, *430*, 195–198. [CrossRef] [PubMed]
7. Lorenz, K.; Lal, R. Effects of Disturbance, Succession and Management on Carbon Sequestration. In *Carbon Sequestration in Forest Ecosystems*; Springer: Dordrecht, The Netherlands, 2010. [CrossRef]
8. Brevik, E.C. Soils and climate change: Gas fluxes and soil processes. *Soil Horiz.* **2012**, *53*, 12–23. [CrossRef]
9. Yazdanpanah, N.; Mahmoodabadi, M.; Cerdà, A. The impact of organic amendments on soil hydrology, structure and microbial respiration in semiarid lands. *Geoderma* **2016**, *266*, 58–65. [CrossRef]
10. Błońska, E.; Lasota, J.; Piaszczyk, W.; Wiecheć, M.; Klamerus-Iwan, A. The effect of landslide on soil organic carbon stock and biochemical properties of soil. *J. Soils Sediments* **2018**, *18*, 2727–2737. [CrossRef]
11. Booth, A.M.; Buma, B.; Nagorski, S. Effects of landslides onterrestrial carbon stocks with a coupledgeomorphic-biologic model: SoutheastAlaska, United States. *J. Ofgeophysical Res. Biogeosci.* **2023**, *128*, e2022JG007297. [CrossRef]
12. Clark, K.E.; West, A.J.; Hilton, R.G.; Asner, G.P.; Quesada, C.A.; Silman, M.R.; Saatchi, S.S.; Farfan-Rios, W.; Martin, R.E.; Horwath, A.B.; et al. Storm-triggered landslides in the Peru-vian Andes and implications for topography, carbon cycles, and biodiversity. *Earth Surf. Dyn.* **2016**, *4*, 47–70. [CrossRef]
13. Vascik, B.A.; Booth, A.M.; Buma, B.; Berti, M. Estimated amounts and rates of carbon mobilized by landsliding in old-growth temperate forests of SE Alaska. *J. Geophys. Res. Biogeosci.* **2021**, *126*, e2021JG006321. [CrossRef]
14. Wang, J.; Jin, Z.; Hilton, R.G.; Zhang, F.; Li, G.; Densmore, A.L.; Gröcke, D.R.; Xu, X.; West, A.J. Earthquake-triggered increase in biospheric carbon export froma mountain belt. *Geology* **2016**, *44*, 471–474. [CrossRef]
15. Ramos Scharrón, C.E.; Castellanos, E.J.; Restrepo, C. The transfer of modern organic carbon by landslide activity in tropical montane ecosystems. *J. Geophys. Res. Biogeosci.* **2012**, *117*. [CrossRef]
16. Błońska, E.; Lasota, J.; Zwydak, M.; Klamerus-Iwan, A.; Gołąb, J. Restoration of forest soil and vegetation 15 years after landslides in a lower zone of mountains in temperate climates. *Ecol. Eng.* **2016**, *97*, 503–515. [CrossRef]
17. Van Oost, K.; Six, J. Reconciling the paradox of soil organic carbon erosion by water. *Biogeosciences* **2023**, *20*, 635–646. [CrossRef]
18. Lal, R. Accelerated soil erosion as a source of atmospheric CO_2. *Soil Tillage Res.* **2019**, *188*, 35–40. [CrossRef]
19. Piaszczyk, W.; Lasota, J.; Gaura, G.; Błońska, E. Effect of Deadwood Decomposition on the Restoration of Soil Cover in Landslide Areas of the Karpaty Mountains, Poland. *Forests* **2021**, *12*, 237. [CrossRef]
20. Schimel, D.S. Terrestrial ecosystem and the carbon cycle. *Glob. Chang. Biol.* **1995**, *1*, 77–91. [CrossRef]
21. Lal, R. Forests soil and carbon sequestration. *For. Soils Carbon Sequestration* **2005**, *220*, 242–258. [CrossRef]
22. Page, S.E.; Siegert, F.; Rieley, J.O.; Boehm, H.D.V.; Jaya, A.; Limin, S. The amount of carbon released from peat and forest ires in Indonesia during 1997. *Nature* **2002**, *420*, 61–65. [CrossRef]
23. Goyal, D.; Joshi, V.; Gupta, N.; Cabral-Pinto, M.M.S. Soil Quality Assessment in a Landslide Chronosequence of Indian Himalayan Region. *Land* **2022**, *11*, 1819. [CrossRef]
24. Chen, S.; Hua, J.; Liu, W.; Yang, S.; Wang, X.; Ji, W. Effects of Artificial Restoration and Natural Recovery on Plant Communities and Soil Properties across Different Temporal Gradients after Landslides. *Forests* **2023**, *14*, 1974. [CrossRef]
25. Nicia, P.; Bejger, R.; Sterzyńska, M.; Zadrożny, P.; Parzych, P.; Bieda, A.; Kwartnik-Pruc, A. Recovery in soil cover and vegetation structure after ancient landslide in mountain fens under Caltho-Alnetum community and response of soil microarthropods (Hexapoda: Collembola) to natural restoration process. *J. Soils Sediments* **2019**, *20*, 714–722. [CrossRef]
26. Pang, D.; Xu, H. Carbon Sequestration and Stability and Soil Erosion in Forest Ecosystems. *Forests* **2024**, *15*, 1961. [CrossRef]
27. Kang, D.; Li, Y.; Ma, L.; Zou, S. Landslide scales affect soil organic carbon accumulation by influencing microbial decomposition of plant-derived carbon after earthquakes. *Ecol. Indic.* **2023**, *155*, 110949. [CrossRef]
28. Pandey, H.P.; Gnyawali, K.; Dahal, K.; Pokhrel, N.P.; Maraseni, T.N. Vegetation loss and recovery analysis from the 2015 Gorkha earthquake (7.8 Mw) triggered landslides. *Land Use Policy* **2022**, *119*, 106185. [CrossRef]
29. Cox, C. Carbon Loss from Earthquake Induced Landslides in Fiordland. *Pūhau Tailwinds* **2024**, *2*, 2. [CrossRef]
30. Frith, N.V.; Hilton, R.G.; Howarth, J.D.; Gröcke, D.R.; Fitzsimons, S.J.; Croissant, T.; Wang, J.; McClymont, E.L.; Dahl, J.; Densmore, A.L. Carbon export from mountain forests enhanced by earthquake-triggered landslides over millennia. *Nat. Geosci.* **2018**, *11*, 772–776. [CrossRef]
31. Peduzzi, P. Landslides and vegetation cover in the 2005 North Pakistan earthquake: A GIS and statistical quantitative approach. *Nat. Hazards Earth Syst. Sci.* **2010**, *10*, 623–640. [CrossRef]

32. Niraj, K.C.; Singh, A.; Shukla, D.P. Effect of the Normalized Difference Vegetation Index (NDVI) on GIS-Enabled Bivariate and Multivariate Statistical Models for Landslide Susceptibility Mapping. *J. Indian Soc. Remote Sens.* **2023**, *51*, 1739–1756. [CrossRef]
33. Shahabi, H.; Hashim, M. Landslide susceptibility mapping using GIS-based statistical models and Remote sensing data in tropical environment. *Sci. Rep.* **2015**, *5*, 9899. [CrossRef] [PubMed]
34. Sevgen, E.; Kocaman, S.; Nefeslioglu, H.A.; Gokceoglu, C. A novel performance assessment approach using photogrammetric techniques for landslide susceptibility mapping with logistic regression, ANN and random forest. *Sensors* **2019**, *19*, 3940. [CrossRef] [PubMed]
35. Peruccacci, S.; Gariano, S.L.; Melillo, M.; Solimano, M.; Guzzetti, F.; Brunetti, M.T. The ITAlian rainfall-induced LandslIdes CAtalogue, an extensive and accurate spatio-temporal catalogue of rainfall-induced landslides in Italy. *Earth Syst. Sci. Data* **2023**, *15*, 2863–2877. [CrossRef]
36. IFFI. IFFI—Inventory of Landslides in Italy (isprambiente.it). Available online: https://idrogeo.isprambiente.it/app/pir?@=41.55172525858242,12.573501484000001,1 (accessed on 30 July 2024).
37. Hungr, O.; Leroueil, S.; Picarelli, L. The Varnes classification of landslide types, an update. *Landslides* **2014**, *11*, 167–194. [CrossRef]
38. Varnes, D.J. Slope Movement Types and Processes. *Spec. Rep.* **1978**, *176*, 11–33.
39. Triggering and Propagation of Rapid Flow-like Landslides—The Proceedings of the Second JTC-1 Workshop—The Landslide Blog—AGU Blogosphere. Available online: https://blogs.agu.org (accessed on 20 October 2024).
40. Larsen, M.C. Rainfall-triggered landslides, anthropogenic hazards, and mitigation strategies. *Adv. Geosci.* **2008**, *14*, 147–153. [CrossRef]
41. Colombo, A.; Lanteri, L.; Ramasco, M.; Troisi, C. Systematic GIS-based landslide inventory as the first step for effective landslide-hazard management. *Landslides* **2005**, *2*, 291–301. [CrossRef]
42. Apip; Takara, K.; Yamashiki, Y.; Sassa, K.; Ibrahim, A.B.; Fukuoka, H. A distributed hydrological–geotechnical model using satellite-derived rainfall estimates for shallow landslide prediction system at a catchment scale. *Landslides* **2010**, *7*, 237–258. [CrossRef]
43. Conforti, M.; Muto, F.; Rago, V.; Critelli, S. Landslide inventory map of north-eastern Calabria (South Italy). *J. Maps* **2013**, *10*, 90–102. [CrossRef]
44. Evaluating the Pre and Syn-Collapse Conditions of Rainfall-Triggered Landslides in Indonesia: Steps Toward Improved Forecasting—Envision—Developing Next Generation Leaders in Environmental Science. Available online: https://www.envision-dtp.org/2023/evaluating-the-pre-and-syn-collapse-conditions-of-rainfall-triggered-landslides-in-indonesia-steps-toward-improved-forecasting/ (accessed on 20 October 2024).
45. Loche, M.; Alvioli, M.; Marchesini, I.; Bakka, H.; Lombardo, L. Landslide susceptibility maps of Italy: Lesson learnt from dealing with multiple landslide types and the uneven spatial distribution of the national inventory. *Earth-Sci. Rev.* **2022**, *232*, 104125. [CrossRef]
46. Application Landslides Archives—Sisgeo. Available online: https://sisgeo.com/category/applications/landslides/ (accessed on 20 October 2024).
47. Slow-Moving Landslides Are a Growing Threat to Mountain Communities, Say Researchers | Technology Networks. Available online: https://www.technologynetworks.com/applied-sciences/news/slow-moving-landslides-are-a-growing-threat-to-mountain-communities-say-researchers-391105 (accessed on 20 October 2024).
48. Guerricchio, A.; Simeone, V. Preliminary remarks on gravitational tectonic deformations and DSGSD in mount Poro headland (Calabria—South Italy). *Rend. Online Soc. Geol. Ital.* **2012**, *21*, 370–371.
49. Deep-Seated Landslide on Mountain in Sehara, Kihō, Beside of Kumano River between Wakayama and Mie Japan Caused by Torrential Rain of Tropical Storm Talas. 2011. Available online: https://www.unsustainablemagazine.com/landslide-prevention/ (accessed on 20 October 2024).
50. Flood in Emilia-Romagna in May 2023, Cartographic Services to Support Emergency Management and Reconstruction Activities—Geoportale. Available online: https://geoportale.regione.emilia-romagna.it/approfondimenti/emergenza-maggio-23/emergenza-rer-maggio-2023-servizi (accessed on 15 October 2024).
51. Huang, F.; Zhang, J.; Zhou, C.; Wang, Y.; Huang, J.; Zhu, L. A deep learning algorithm using a fully connected sparse autoencoder neural network for landslide susceptibility prediction. *Landslides* **2020**, *17*, 217–229. [CrossRef]
52. Mahalingam, R.; Olsen, M.J. Evaluation of the influence of source and spatial resolution of DEMs on derivative products used in landslide mapping. *Geomat. Nat. Hazards Risk* **2016**, *7*, 1835–1855. [CrossRef]
53. Gorelick, N.; Hancher, M.; Dixon, M.; Ilyushchenko, S.; Thau, D.; Moore, R. Google Earth Engine: Planetary-scale geospatial analysis for everyone. *Remote Sens. Environ.* **2017**, *202*, 18–27. [CrossRef]
54. Jin, Z.; Azzari, G.; You, C.; Di Tommaso, S.; Aston, S.; Burke, M.; Lobell, D.B. Smallholder maize area and yield mapping at national scales with Google Earth Engine. *Remote Sens. Environ.* **2019**, *228*, 115–128. [CrossRef]
55. Prakash, N.; Manconi, A.; Loew, S. Mapping landslides on EO data: Performance of deep learning models vs. Traditional machine learning models. *Remote Sens.* **2020**, *12*, 346. [CrossRef]
56. Trigila, A.; Iadanza, C.; Spizzichino, D. Quality assessment of the Italian Landslide Inventory using GIS processing. *Landslides* **2010**, *7*, 455–470. [CrossRef]
57. Kavzoglu, T.; Sahin, E.K.; Colkesen, I. An assessment of multivariate and bivariate approaches in landslide susceptibility mapping: A case study of Duzkoy district. *Nat. Hazards* **2015**, *76*, 471–496. [CrossRef]

58. Kellner, J.R.; Armston, J.; Duncanson, L. Algorithm theoretical basis document for GEDI footprint aboveground biomass density. *Earth Space Sci.* **2023**, *10*, e2022EA002516. [CrossRef]
59. Shendryk, Y. Fusing GEDI with earth observation data for large area aboveground biomass mapping. *Int. J. Appl. Earth Obs. Geoinf.* **2022**, *115*, 103108. [CrossRef]
60. 2006 IPCC Guidelines for National Greenhouse Gas Inventories, Volume 4, Agriculture, Forestryand Other Land Use. Available online: https://www.ipcc-nggip.iges.or.jp/public/2006gl/vol4.html (accessed on 20 October 2024).